ADVANCED MATERIALS INTERFACES
Open Access
www.advmatinterfaces.de

Effects of the Polymer Amount and pH on Proton Transport in Mesopores

*Laura Despot and Annette Andrieu-Brunsen**

Proton exchange membranes (PEMs) have various applications, such as in electrolysis technology for hydrogen generation, vanadium flow batteries for energy storage, and fuel cells for energy conversion. To increase PEM performance and expand the range of PEM applications, the underlying transport mechanisms of PEMs need to be understood. Mesoporous silica thin films are versatile model materials for proton transport investigation and are prepared with a pore size of ≈12 nm and film thickness of ≈565 nm by evaporation-induced self-assembly, providing an ordered, mesoporous, rigid matrix that allows us to deduce the structure-property relationship with respect to proton conductivity. Different amounts of sulfonic acid-bearing groups are introduced into the mesopores using the grafting-through polymerization of sulfopropylmethacrylate. The relationship between proton transport and the pH of the surrounding solution in poly-sulfopropylmethacrylate-functionalized mesopores is investigated using electrochemical impedance spectroscopy. The proton conductivity is found to depend on both the proton concentration in solution and the number of proton transporting groups inside the pore, indicating the major role of charge regulation and the confinement effect on proton transport.

1. Introduction

Energy consumption is steadily increasing.[1] Together with climate change, this has resulted in a shift towards more carbon-neutral energy sources. Fuel cells are an attractive alternative for energy conversion because of their high efficiency and lack of pollutant emissions.[2] Based on the reaction of oxygen and hydrogen, an electrical current can be produced, whereas the transport of protons from the anode to the cathode takes place via a PEM that blocks gas transport, which makes the PEM the key component of the cell.[3] The first commercially available and most efficient PEM to date is Nafion.[4] This polymeric membrane became the standard membrane for fuel cells due to the combination of its relatively high thermal and chemical stability and its high ionic conductivity of ≈0.1–0.01 S cm^{-1}.[5] However, applications of Nafion are limited, for example, at temperatures above 100 °C and below 0 °C.[4] These limitations have inspired research on novel PEM materials as well as on understanding and modulating proton transport. Various approaches on polymeric membranes,[6] porous materials,[7] and development of composite materials[8] can be found in the literature. Proton transport through structurally rigid and ordered nanoscale porous materials used as membranes, such as mesoporous silica, is of special interest, as changes in proton conductivity can be directly correlated to the membrane characteristics, factors such as swelling can be excluded, and water management can be facilitated, e.g., profitable condensation can occur. Regarding proton conductivity, mesoporous ceramic materials show important key properties, such as a high specific surface area, stability, and adjustable pore geometries.[9] Due to the high diversity in terms of surface chemistry, mesoporous silica allows a variety of possible functionalization approaches, such as postgrafting,[10] cocondensation[11] or acid impregnation,[12] for improving proton conductivity. Inagaki and coworkers[13] showed that a temperature increase as well as an increase in relative humidity resulted in improved proton conductivity through sulfonic acid-functionalized mesoporous silica films comparable to those observed for Nafion. They also observed an increase in proton conductivity with decreasing pore diameter from 4 nm to 2 nm, which was ascribed to increased water condensation and higher acid density. In particular, the increase in proton conductivity with increasing temperature using sulfonic acid-functionalized porous silica was discussed in different studies,[10b,11a,13,14] and a higher flexibility of organic chains bearing sulfonic acid groups and higher diffusion of water led to an increase in proton conductivity with temperature.

Géradin and coworkers[15] used an in situ mesopore functionalization approach[16] to integrate a polyion electrostatic complex consisting of a sulfonic acid-bearing polyacid-based double-hydrophilic block copolymer and an oppositely charged polyelectrolyte for structure-directing, functionalization, and mesopore generation of mesoporous silica.

L. Despot, A. Andrieu-Brunsen
Ernst-Berl-Institut für Technische und Makromolekulare Chemie
Technische Universität Darmstadt
64289 Darmstadt, Germany
E-mail: annette.andrieu-brunsen@tu-darmstadt.de

The ORCID identification number(s) for the author(s) of this article can be found under https://doi.org/10.1002/admi.202202456.

DOI: 10.1002/admi.202202456

They achieved proton conductivities of up to 0.024 S cm^{-1} at 363 K/95% relative humidity with an environmentally friendly one-shot synthesis procedure.

Zharov and coworkers[17] demonstrated the effect of the sulfonic acid content in colloidal membranes on proton conductivity. A sigmoidal dependence of the content of sulfonic acid groups on the proton conductivity was observed. Furthermore, at a certain point, ion-rich clusters joined together, resulting in a sudden increase in conductivity.

When using pH-responsive mesoporous materials, such as pH-responsive mesoporous silica, the pH of the surrounding solution is known to influence the overall performance. For mesoporous silica films, it has been observed that surface charge-mediated transport is dominant at low proton concentrations, resulting in a pH-independent, constant proton conductivity. At high proton concentrations, proton conductivity is linearly dependent on proton concentration, known as the bulk behavior regime. At the transition between these two regimes, the deprotonation of silanol groups significantly influences proton transport.[18] Bulk and surface charge behavior of mesoporous silica thin films was also reported by Zhao et al.[19] They showed that the measured conductance was at least four times higher than that calculated by theoretical models, indicating the effect of nanoconfinement on proton transport, as this was not considered in the calculations. To the best of our knowledge, studies explaining the pH-dependent proton transport phenomena, not just those dependent upon proton concentration, of additional acid-functionalized mesoporous silica have not yet been reported. Using structurally defined nanochannels is of interest for understanding proton transport under nanoconfinement and for optimizing membrane properties. Additionally, the incorporation of sulfonic acid groups inside the mesoporous structure is inspired by Nafion, as it has sulfonic acid groups that are critical for proton conductivity.[4] In contrast to Nafion, the mesoporous ceramic structure is rigid and cannot swell. A shift from the pKa of polymers in bulk solution toward that of the polymers in mesopores in the context of charge regulation and confinement effects has been reported previously,[20] but the effects on proton conductivity properties are still unexplored.

In this study, we functionalized mesoporous silica films with varying amounts of PSPMA by grafting-through polymerization. We used these mesoporous polymer-functionalized silica films as model materials with high structural order to investigate the confinement effect on proton transport by performing EIS measurements, as they have been used for analyzing transport mechanisms through mesoporous silica.[13,21] By titrating the pH value of the surrounding solution, the pH dependence of proton transport mechanisms was elucidated.

2. Results and Discussion

To investigate the influence of pH and polyelectrolyte density on ion and proton transport in mesopores, mesoporous silica thin films were functionalized with varying amounts of PSPMA (**Figure 1**). The polymerization was carried out by visible light-induced iniferter-initiated polymerization. 4-Cyano-4-((dodecylsulfanylthiocarbonyl)sulfanyl)pentanoic acid (CDTPA) was used as an iniferter in a grafting-through approach according to previous work from John et al.[22] Iniferter-initiated polymerizations did show good control of the polymer amount inside mesopores. Furthermore, iniferter-initiated polymerization allowed polymerization control without adding additional components that must diffuse into the mesopore to allow polymerization control.[23] Mesoporous silica thin films were obtained according to a method adapted from Dunphy et al. as

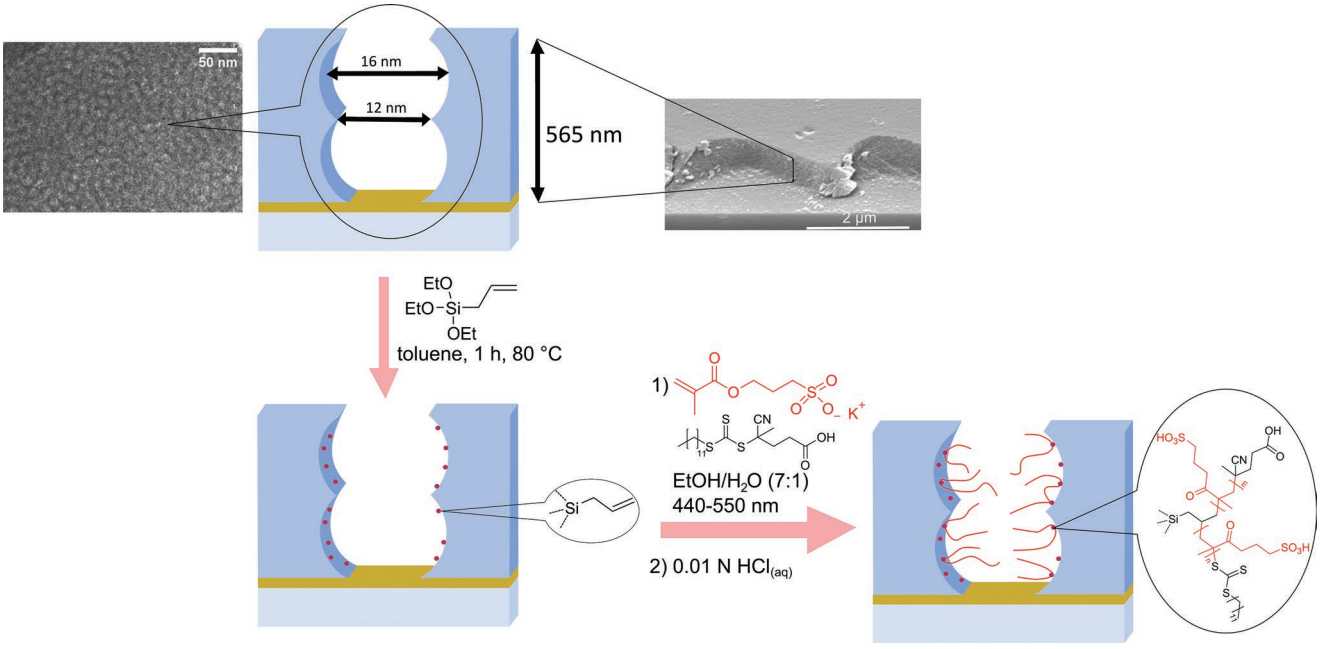

Figure 1. TEM and SEM images of the mesoporous silica film and schematic illustration of the allylsilane and further polymer modification of the silica film using SPMAK as the monomer and CDTPA as the iniferter.

described previously.[24] Due to the assembly of micelles, constrictions occurred at the contact points, resulting in elliptical pores. The narrower part of the pore had a diameter of 12 nm (Figure S1, Supporting Information), and the wider part had a diameter of 16 nm, as determined by TEM, with an average film thickness of 565 nm, as determined by ellipsometry and SEM, corresponding to results reported in previous studies.[20a] The porosity of 62 vol.% was calculated from the refractive indices determined by ellipsometry measurements at 15% relative humidity using the Brüggeman effective medium approximation (Table S1, Supporting Information).[25] To achieve polymer functionalization during grafting, allyltriethoxysilane was covalently bound to the mesoporous silica film. The functionalization with PSPMA was limited to the inner pore wall surface by applying CO_2-plasma treatment to the allyl-functionalized silica films using a protocol according to Babu et al.[26] and removing allyl groups at the outer planar mesoporous silica film surface. Sulfopropylmethacrylate potassium salt (SPMAK) and CDTPA were used for the polymerization, followed by ion exchange in 0.01 M aqueous hydrochloric acid solution to generate the sulfonic acid group.

Since CDTPA absorbs blue light at 440 nm (Figure S2, Supporting Information), irradiation with visible light at 440–550 nm induced a polymerization reaction in a grafting-through process. Successful polymer grafting was indicated by the detection of the PSPMA C=O vibrational band at 1710 cm^{-1} in the ATR-IR spectra obtained by measuring the polymer-functionalized mesoporous silica thin films after scratching them off the substrate. The ATR-IR spectra were normalized to the Si—O–Si stretching vibrational band at 1040 cm^{-1} (**Figure 2**a). The PSPMA amount was gradually adjusted by adjusting the irradiation time of a 1 M SPMAK solution in ethanol/water (7:1) containing 0.0034 equivalents of CDTPA from 10 min to 2.5 h reaction time. Up to an irradiation time of 2.5 h, by evaluating two or three polymerizations for each polymerization time, an increase in the polymer content relative to a C=O vibrational band intensity at 1710 cm^{-1} of 0.043 was observed (Figure 2b). An almost linear monomer conversion with reaction times up to 2.5 h was also observed during polymerization in solution (Figure S3, Supporting Information). This indicates polymerization control suitable for the reproducible adjustment of the polymer amount in the silica mesopores while maintaining an intact porous structure (Figure S4, Supporting Information). In addition, polymer fractions up to 22 wt.% were determined by TGA.

Proton transport was characterized using EIS. EIS measurements were performed in water while the solution pH was titrated from acidic to basic to investigate the correlation between polymer amount and charge regulation in mesopores on the mesoporous film resistance and proton conductivity. To ensure constant pH conditions during the measurement, the pH was monitored before and after EIS measurements using a pH electrode. Polymer stability was tested by performing IR spectroscopy before and after incubation of the PSPMA-functionalized silica film according to the impedance spectroscopy measurement conditions (Figure S6, Supporting Information). **Figure 3**a depicts the experimental 3-electrode setup consisting of a glassy carbon counter electrode, a Ag/AgCl reference microelectrode and a mesoporous thin film on an ITO-covered glass substrate as the working electrode. The equivalent circuit (EC), which was used for fitting the measurements of unfunctionalized and PSPMA-functionalized mesoporous silica films, is displayed in Figure 3b. The EC included a parallel resistance R_s and capacitor C_s representing the surrounding solution, a pore resistance R_{pore} in series with the polymer resistance $R_{polymer}$ and a constant phase element CPE_{dl} representing the electrical double-layer at the electrode-water interface (as described by Bisquert[26]) and a pore wall capacitor $C_{pore\ wall}$. This EC was used for analyzing the nonfunctionalized silica films as well as the silanol groups on the film surface. For the allyl-functionalized silica film, the EC shown in Figure 3c was used. The more hydrophobic surface due to the incorporation of the organic hydrophobic allyl groups resulted in a decreasing amount of water inside the pores and thus in less water-driven proton transport. Additionally, due to the decrease in the number of silanol groups or the absence of an additional proton-conducting functional group, such as sulfonic acid groups, the EC was adjusted by removing $R_{polymer}$ and CPE_{dl}, representing the functional groups attached to the surface.

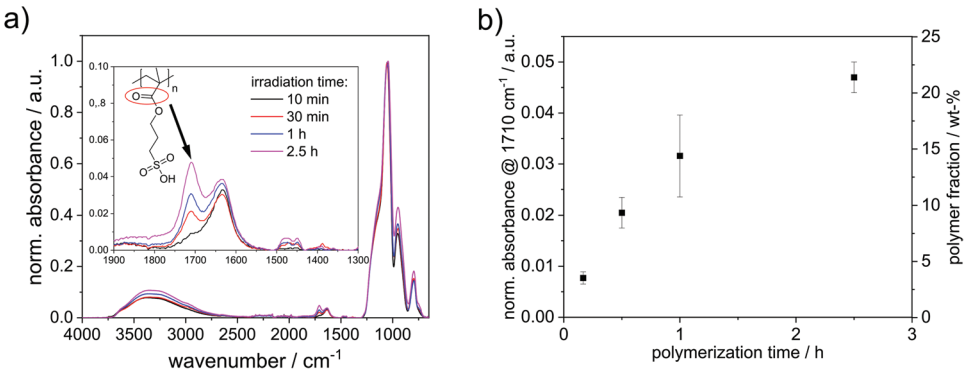

Figure 2. a) Normalized ATR-IR spectra of scratched PSPMA-functionalized silica films after different irradiation times. Background and baseline correction were automatically applied by Spectrum software (Version 10.5.4) from PerkinElmer. Spectra were normalized to the Si—O–Si-vibration at 1045 cm^{-1} using the software OriginPro9. b) C=O absorbance at 1710 cm^{-1} attributed to PSPMA in the pores observed in a series of 2-3 polymerizations and polymer fraction determined with TGA against irradiation time. All results are shown as the mean of two to three replicates ± standard errors of the means.

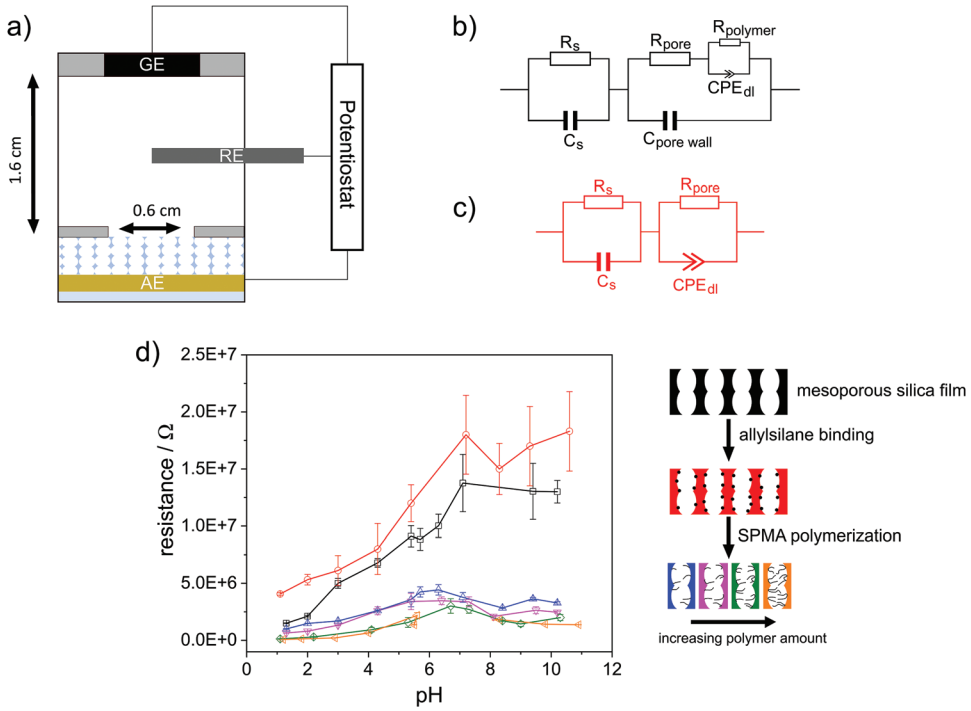

Figure 3. a) Experimental 3-electrode setup consisting of a glassy-carbon counter electrode, a Ag/AgCl reference microelectrode, and a mesoporous thin film on an ITO-covered glass substrate as a working electrode. b) Equivalent circuit used for fitting the impedance data of mesoporous silica film and PSPMA-functionalized silica films. c) Equivalent circuit used for fitting the impedance data of allyl-functionalized silica films. d) Fitted resistances of mesoporous silica films on the ITO electrode against the pH of the surrounding solution. Data are presented as fitted resistance ± error calculated for the parameter using RelaxIS 3 from rhd instruments.

In general, the resistance of the mesoporous silica film (denoted by the black data points in Figure 3d) increased after incorporating allyl groups (Figure 3d red). This was expected, as the number of available silanol groups is reduced, the pore volume is slightly reduced and the pore wall became slightly more hydrophobic. Assuming the occurrence of the Grotthus mechanism as it is indicated by temperature-dependent impedance studies (Figure S7, Supporting Information) and thus proton hopping along hydrogen-bonded water molecule chains or acidic groups,[4] an increasing resistance was expected upon allyltriethoxysilane functionalization. As expected upon incorporation of the sulfonic acid groups using grafting-through PSPMA, the pore resistance range decreased from the range of 4.1×10^6—2×10^7 Ω to the range of 1.0×10^6–3.3×10^6 Ω over the entire pH range (Figure 3d, red and blue), clearly showing facilitated proton transport. A further slight decrease in resistance range from the range of 1.0×10^6–3.3×10^6 Ω to the range of 8×10^4–1.5×10^6 Ω was observed when increasing the PSPMA fraction from 3 to 22 wt.% (Figure 3d, blue and orange). This significantly decreasing resistance for low pore-filling degrees compared to that of the polymer-free mesoporous film indicates a strong influence of the ionic group presence on proton transport.

In addition to polymer functionalization, proton conductivity is significantly influenced by the solution pH. In the case of unfunctionalized, allyltriethoxysilane- and PSPMA-functionalized mesoporous silica films, two distinct pH ranges were identified. At more acidic pH values for unmodified and allyltriethoxysilane-functionalized mesoporous silica films, an almost linear increase in resistance with increasing pH until a solution pH of approximately seven was observed. In this pH range below seven, the functional silanol groups at the mesopore walls were protonated. Under these conditions, the decreasing proton concentration in the solution with increasing pH as pH = –lg (proton concentration)[27] was probably the detrimental factor for the increasing resistance. At pH 7, a maximum resistance was detected, which did not increase further even when increasing the solution pH and thus decreasing the solution proton concentration. This indicates the detrimental role of the pKa value of the pore wall silanol groups, which were deprotonated at this pH, causing an additional preconcentration of ionic species and probably an increased number of protons inside the pore. Reproducibility experiments showing the same trend are shown in Figure S8, Supporting Information, for two unfunctionalized mesoporous silica films and PSPMA-functionalized silica films with seven different polymer amounts. It must be noted that due to the high sensitivity of EIS, even slight deviations in the polymer amount, in the silica film properties, or in the pretreatment led to changes in the absolute values of resistance and conductivity, as demonstrated systematically in our previous study.[29] Nevertheless, the trend toward lower resistances with increasing PSPMA amount was clearly and reproducibly identified.

It must be noted that the pH of maximum resistance and thus the transition point from pH-dominated resistance to constant resistance governed by the amount of polyelectrolyte within the mesopores shifted approximately one pH value toward acidic pH upon PSPMA grafting (Figure 3d

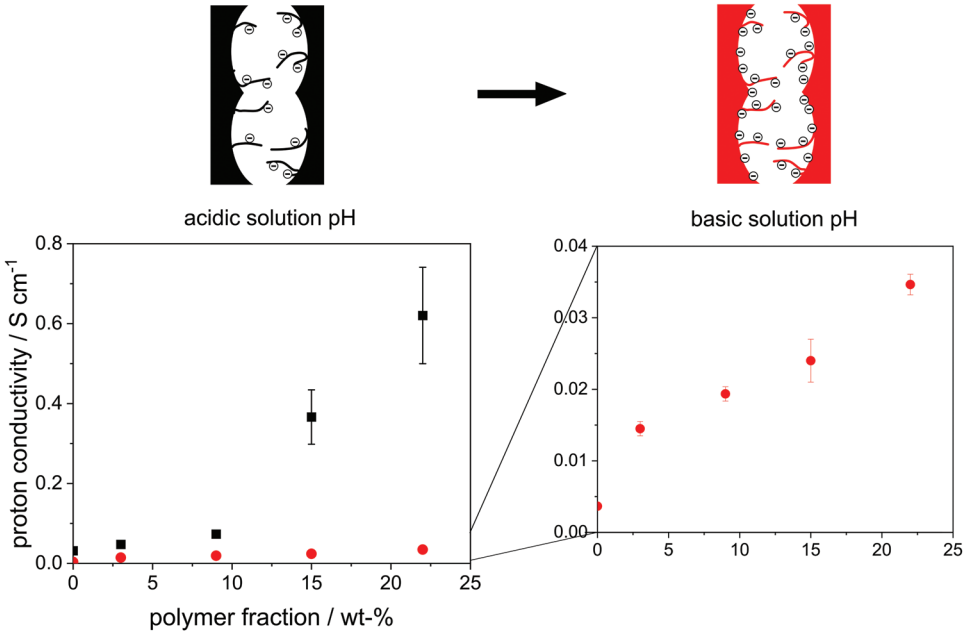

Figure 4. Proton conductivity of unfunctionalized (0 wt-% PSPMA) and PSPMA-functionalized mesoporous silica film as a function of the polymer weight fraction at solution pH values of 1 and 10. Proton conductivity was calculated by $\sigma = L/RA$ using fitted resistances and sample and setup dimensions. Data are presented as calculated proton conductivity ± error calculated via the propagation of uncertainty using the errors from fitting impedance data using RelaxIS 3 from rhd instruments.

black, blue). Upon further increase of the polymer amount, a certain polymer amount increase again shifted this transition pH from 6.5 to 7.5 (Figure 3d blue and pink versus green and yellow). This trend may also be indicated in Figure S5b, Supporting Information, and is in accordance with pKa shifts in confinement. It is well known that spatial confinement strongly influences charge regulation in nanopores.[20,30] This was also shown by cyclic voltammetry measurements collected while titrating the pH value of the mesopore surrounding solution, where a pKa value of 8.5 ± 0.1 for the silanol groups of the mesoporous silica films applied here and 7.5 ± 0.5 for PSPMA in these mesoporous silica films were obtained (Figure S9, Supporting Information). The pKa value of 8.5 was mainly attributed to geminal silanol groups or vicinal silanol groups.[31] Stabilization through hydrogen bonds increased the pKa value in comparison to that of the isolated silanol groups. The decreased pKa value of 7.5 for PSPMA-functionalized silica films was ascribed to a mixture of the silanol groups on the silica surface and the sulfonic acid groups of the polymer. The pKa values of polymers in solution containing sulfonic acid groups were reported to be in the range of 2–3.[32] Cyclic voltammetry measurements of a PSPMA-functionalized silica film showed that an anionic probe molecule was excluded at acidic as well as at basic pH (Figure S10, Supporting Information), demonstrating the pH-independent negative charge of the sulfonic acid groups inside the pores in the mentioned pH range.

Based on the resistance R discussed thus far, the proton conductivity was calculated according to the relation $\sigma = L/RA$,[33] where L = 1.6 cm is the length of the solvent chamber and A = 0.6 cm × 560 nm (width × membrane thickness) is the area available for proton transport. The results showed an increase in the proton conductivity upon incorporating sulfonic acid into the mesopores up to the range of Nafion[5] (compare to Figure S11: proton conductivity at neutral solution pH). **Figure 4** shows the proton conductivity for mesoporous silica films without and with increasing amounts of PSPMA. The corresponding impedance spectra are shown in Figure S12, Supporting Information. As expected at acidic solution pH (Figure 4, black data points), the proton conductivity was up to 18 times higher than at basic solution pH (Figure 4, red data points) comparing the results with the highest PSPMA amount of 22 wt.% and the proton conductivities of 0.62 S cm^{-1} and 0.035 S cm^{-1}. Since proton conductivity was highly dependent on the amount of protonic charge carriers, the small amount of proton charge carriers in solution at basic pH led to low proton conductivity. The high proton conductivities at pH 1 were mainly attributed to the high proton concentration in solution, as is the case in the bulk behavior regime. At acidic solution pH, a small sulfonic acid group content had a small effect on proton conductivity when comparing polymer fractions below and above 10–15 wt.%. When increasing the polymer fraction above 10–15 wt.%, there was a significant dependence of proton conductivity on the polymer fraction (Figure 4). This notable increase in proton conductivity upon reaching 10–15 wt.% PSPMA could be explained by the exceeding of a critical amount of sulfonic acid groups that contribute significantly to proton transport. This threshold was not observed at basic solution pH. At basic pH, the proton conductivity was almost linearly dependent on the polymer amount starting at the lowest polymer content. This pH influence indicates the notable influence of the generated charge inside the pores in addition to the proton concentration in solution.

3. Conclusion

To investigate the polymer amount and solution pH dependence of proton transport using EIS, sulfonic acid groups carrying PSPMA are incorporated into mesoporous silica films, achieving a PSPMA polymer fraction of up to 22 wt.%. Proton transport in mesopores is affected by both the proton concentration in solution (solution pH) and mesopore charge and thus mesopore wall polymer functionalization. For solution pH values below the pKa, resistance increases with increasing pH and thus decreasing proton concentration. For solution pH values above the pKa, the resistance remains constant, indicating a pH-independent charge within the mesopores in this solution pH range that governs the proton conductance. As expected, charge regulation and thus the pKa inside these mesopores influence resistance. Upon PSPMA functionalization, the pH of maximum resistance shifts to 6.5, whereas it shifts even further to 7.5 upon introducing a critically higher polymer amount of up to 22 wt.%. Introducing the polyelectrolyte PSPMA leads to a significant decrease in resistance at relatively low polymer amounts. A further increase in PSPMA inside the pores further decreases the resistance to a minimum value of 76 600 Ω observed in our study at an acidic pH. The absolute values of proton conductivity of PSPMA-functionalized mesopores are comparable to the proton conductivity of Nafion. Proton conductivity increases with increasing PSPMA amount at acidic pH. This indicates that the proton conductivity is mainly dependent on the number of acid groups inside the pores, although the proton concentration in solution must also be considered. Upon changing the pH to basic conditions far beyond the pKa of PSPMA-functionalized mesopores, proton conductivity strongly decreases from 0.62 S cm^{-1} at acidic pH to 0.035 S cm^{-1} at basic pH compared to that of the samples with the highest PSPMA amount of 22 wt.%. Nevertheless, proton conductivity clearly shows a polymerization time and thus polymer amount dependence. The proton conductivity increases by a factor of ≈1.3 from 14.5 mS cm^{-1} to 19.4 mS cm^{-1}, 24.0 mS cm^{-1} and 34.7 mS cm^{-1} at basic pH with increasing polymer amount from 3 wt.% to 9 wt.%, 15 wt.%, and 22 wt.%, respectively. Consequently, this study provides design criteria for proton-conducting nanopores and membranes. In addition, ceramic membranes might be of interest for proton transport, especially as water management might already be achieved using water vapor at vapor pressure, allowing condensation inside the pores.

4. Experimental Section

Materials: Pluronic F127, Emplura ethanol, 3-sulfopropyl methacrylate potassium salt (98 %), and 4-cyano-4-[(dodecylsulfanylthiocarbonyl) sulfanyl]pentanoic acid (97 %, HPLC grade) were purchased from Sigma Aldrich. Tetraethoxysilane (98%) and triethylallylsilane (97 %) were received from Alfar Aesar, and toluene (Rotidry, ≤50 ppm H_2O) was obtained from Carl Roth. All chemicals were used as received unless noted otherwise.

Preparation of Mesoporous Silicafilm: For the synthesis of mesoporous silica thin films with pore sizes of 10–16 nm, a sol-gel solution with the following molar ratios of TEOS : F127 : H2O : ethanol : HCl (37%) was used in accordance with a method adapted from Dunphy et al.[24]: 1 : 0.01 : 17 : 20 : 0.015. Briefly, TEOS (9.8 mL, 44.22 mmol) was dissolved in 48.0 mL of EtOH (822.05 mmol). Then, 5.22 g of F127 (0.41 mmol) was added under stirring. Finally, 12.8 mL 0.05 M HCl (0.64 mmol) was added. The solution was stirred for 20 min before dip-coating to produce thin films at a withdrawal speed of 2 mm s^{-1}, a relative humidity (RH) of ≈50 % and a temperature of ≈25 °C. Prior to dip-coating, the substrate (glass and ITO-covered glass) was H_2O-plasma treated at a pressure of 0.2–1 mbar and a power of 10 % (10 Watt) for 10 min using a Diener Electronic Femto plasma oven to activate the surface and ensure better adhesion of the silica film. Freshly deposited films were kept under these climate conditions for at least 1 h before being thermally treated with the following oven program: 1 h at 60 °C and 1 h at 130 °C followed by heating to 350 °C with a heating rate of 1 °C min^{-1} and stabilization at 350 °C for 2 h.

Surface Functionalization with Allyltriethoxysilane: The mesoporous silica thin film substrate was placed into a polymerization flask under N_2 atmosphere and covered with 20 mL of a 1 mM solution of allyltriethoxysilane (4.5 µL, 5.5 mg, 0.025 mmol) in dry toluene (20 mL). The functionalization was conducted in a water bath at 80 °C for one hour. Hereafter, the substrates were extracted in a beaker filled with sufficient toluene to cover the whole substrate. The substrate was left for 15 min, rinsed with 10 mL ethanol, and dried under ambient conditions. To remove the functional groups on the outer surface, the substrates were CO_2 plasma treated at a pressure of 0.3 mbar and a power of 20% (10 Watt) for 12 s using a Diener Electronic 20 Femto plasma oven according to a protocol reported in the literature.[25]

PSPMA Modification of Pore Surface by a Grafting-Through Process: Briefly, 7.576 g (30 mmol, resulting concentration: 1 M, 1 Eq.) sulfopropylmethacrylate potassium salt 98% 30 mL EtOH/H2O (7:1, 26.2 mL EtOH, 3.8 mL H2O) and 44.2 mg 4-Cyano-4-[(dodecylsulfanylthiocarbonyl)sulfanyl]pentanoic acid (102 µmol, 0.0034 Eq) were mixed in a round flask. For 15 min, N_2 was bubbled through the solution before the solution was poured in cuvettes containing allyl-functionalized silica films on glass or ITO-covered glass. The irradiation times for the polymerizations using a Lumatec lamp superlite 400 (Filter 6: 12 mW cm^{-2}) were selected between 10 min and 2.5 h. The substrates were extracted in water for 10 min and in ethanol for 20 min using a beaker filled with sufficient solvent to cover the whole substrate. Then, ion exchange was conducted in a beaker filled with sufficient 0.01 M HCl solution to submerge the entire silica film for a maximum time of 45 min. Then, ion exchange took place in a beaker filled with enough 0.01 M HCl solution to submerge the entire silica film for a maximum time of 45 min.

ATR-IR Spectroscopy: Infrared spectra of the mesoporous films were recorded using a PerkinElmer Spectrum One FT-IR spectrometer. The films were scratched off the substrate before measurements were performed. The spectra were recorded from 4000 to 650 cm^{-1} with a resolution of 4 cm^{-1} using Spectrum software (Version 10.5.4) by PerkinElmer. The background and baseline corrections were automatically applied. Normalization to the Si–O–Si vibration at 1045 cm^{-1} was conducted using OriginPro9 software.

Ellipsometry: Ellipsometry measurements for determining the layer thickness of mesoporous silica films were carried out using the Accurion Nanofilm EP3 ellipsometer. The measurements were carried out with angles of incidence between 38° and 68° at a step size of 2° at three measuring positions along the withdrawal direction of the dip coating. Measurements were taken in one-zone mode. For the evaluation, a single-layer model of the mesoporous films of silicon substrates (Si wafer, SiO_2 layer, SiO_2 mesoporous) was created with the program EP4-Model (version 1.2.0) from Accurion to describe the surface using fitting limits of 400–600 nm for film thickness and 1.0–1.5 for refractive index. Using a humidity controller and the program Regul'Hum (version 3.3) from SolGelWay, the relative humidity was kept at 15 %.

UV–Vis-Spectroscopy: UV–Vis spectroscopy was performed on an Agilent Cary 60 UV–Vis spectrophotometer. The investigated wavelength range was 350 nm to 800 nm. All measurements were performed in PMMA plastic cuvettes (Brand) with a cuvette path length of 1 cm.

SEM: A scanning electron microscope ZEISS DSM 962 with an SE detector was used (resolution: 10 nm lateral). The samples were cut

to size and glued to a sample holder with a carbon film. For cross-sectional imaging, the samples were fixed with a conductive tape strip. The samples were covered with a 7 nm thick layer of Pd/Pt alloy using a Cression 208 HR sputter coater.

TEM: Transmission electron micrographs were recorded by Ulrike Kunz (Material Science) using a Philips FEI CM20 transmission electron microscope equipped with a LAB-6 cathode and Olympus CCD camera operating at an accelerating voltage of 200 kV. For the examination of the porous silica films, the samples were scraped off and suspended in ethanol. Before placing one drop on a TEM mesh, they were treated for 5–10 min in an ultrasonic bath.

Cyclic Voltammetry: CV measurements while titrating the solution pH were carried out according to Brilmayer et al.[20a] The CV measurements were recorded using an Autolab PGSTAT302N potentiostat from Metrohm. An anionic probe molecule $[Fe(CN)_6]^{4-/3-}$ and a cationic probe molecule $[Ru(NH_3)_6]^{2+/3+}$ (each 1 mM in phosphate buffer solution: 8.00 g (136.9 mmol) NaCl, 0.20 g (2.7 mmol) KCl, 1.42 g Na_2HPO_4 (10.0 mmol), 0.27 g (2.0 mmol) KH_2PO_4 in 1000 mL water) were used. The indium tin oxide layer of the respective substrates supporting the mesoporous film (Delta Technologies, resistance of 4–8 Ω) served as the working electrode. A Ag/AgCl electrode (BASi RE-6) served as the reference electrode, and a graphite electrode served as the counter electrode. The pH-dependent mesopore accessibility was investigated by adjusting the solution pH between pH 2 and pH 11 by adding hydrochloric acid and sodium hydroxide solution using a pH-meter Seven Compact S220 by Mettler Toledo. The measurements with $[Fe(CN)_6]^{4-/3-}$ were carried out at a voltage of –0.2 V to 0.6 V, and the measurements with $[Ru(NH3)_6]^{2+/3+}$ were carried out at a voltage of -0.6 V to 0.3 V. Measurements were taken at scan rates of 200 mV s^{-1}, 100 mV s^{-1}, 25 mV s^{-1}, 300 mV s^{-1}, 500 mV s^{-1} and finally again at 200 mV s^{-1}. Three cycles were run at each scan rate to ensure that equilibrium had been reached. For the evaluation, a scan rate of 100 mV s^{-1} was considered in each case. After including the electrode surface area (0.21 cm^{-2}), the current density J in µ A cm^{-2} was plotted against the potential *E* in V.

Electrochemical Impedance Spectroscopy: Transverse EIS measurements were carried out using a Metrohm Autolab PGSTAT204 potentiostat with an FRA32M module in combination with Nova2 Software and the measuring cell TSC surface from rhd instruments with their electrodes at room temperature. In the three-electrode setup, a Ag/AgCl microelectrode served as a reference electrode, glassy carbon served as a counter electrode and the mesoporous thin film on a conductive ITO substrate (Delta technology) served as the working electrode. The impedance was measured over a frequency between 0.1 Hz and 1 MHz (for pH ≈1: 0.1 Hz to 100 kHz) with an amplitude of 10 mV. The data analysis for the EI spectra was performed with the software RelaxIS 3 from rhd instruments by fitting to the equivalent circuit shown in Figure 3. The measurements were performed in water. To investigate the dependence of the pH value of the solution on the impedance and thus the proton transport, the pH of the surrounding solution was adjusted using hydrochloric acid and sodium hydroxide solution and a pH-meter Seven Compact S220 by Mettler Toledo. To investigate the temperature dependence the measuring cell was heated up in a climate chamber from 30 °C to 60 °C in steps of 10 °C respectively. The temperature was held for 2 h before the measurement.

Statistical Analysis: For IR analysis, the arithmetic means (averages) and standard errors of the means of two to three replicates were used as measures of center and spread. Resistances resulting from impedance measurements were fitted using RelaxIS 3 from rhd instruments with errors calculated by the software. Proton conductivity data are shown as calculated proton conductivity ± error calculated via propagation of uncertainty. In all cases, no data points were excluded as outliers.

Supporting Information

Supporting Information is available from the Wiley Online Library or from the author.

Acknowledgements

The authors kindly acknowledge the financial support by the German Research Foundation (DFG) within the Collaborative Research Centre 1194 "Interaction between Transport and Wetting Processes", Project-ID 265191195, subprojects C04 and by the Rhein-Main University collaboration. In addition, the authors wish to thank C. Karlsson (rhd instruments GmbH & Co. KG) for temperature-dependent impedance measurements, U. Kunz for TEM imaging, and Prof. M. Biesalski for access to analytic equipment and infrastructure.

Open access funding enabled and organized by Projekt DEAL.

Conflict of Interest

The authors declare no conflict of interest.

Data Availability Statement

The data that support the findings of this study are available from the corresponding author upon reasonable request.

Keywords

electrochemical impedance spectroscopy, mesoporous silica thin films, pH-dependent proton transport, polyelectrolyte

Received: December 12, 2022
Revised: March 17, 2023
Published online: April 18, 2023

[1] S. Dale, *bp Statistical Rev. World Energy* **2022**, https://www.bp.com/en/global/corporate/energy-economics/statistical-review-of-world-energy.html.
[2] M. Z. Jacobson, W. G. Colella, D. M. Golden, *Science* **2005**, *308*, 1901.
[3] M. Winter, R. J. Brodd, *Chem. Rev.* **2005**, *105*, 1021.
[4] A. Kusoglu, A. Z. Weber, *Chem. Rev.* **2017**, *117*, 987.
[5] S. Slade, S. A. Campbell, T. R. Ralph, F. C. Walsh, *J. Electrochem. Soc.* **2002**, *149*, 1556.
[6] a) S. D. Mikhailenko, M. A. S. Rodrigues, F. Celso, F. Muller, C. A. Ferreira, S. Kaliaguine, *J. Phys. Chem. B* **2018**, *122*, 7764; b) V. Vijayakumar, K. Kim, S. Y. Nam, *Appl. Chem. Eng.* **2019**, *30*, 643.
[7] a) A. Gupta, S. Goswami, S. M. Elahi, S. Konar, *Cryst. Growth Des.* **2021**, *21*, 1378; b) J. Zhang, S. P. Jiang, in *Nanomaterials For Sustainable Energy*, Springer, Cham **2016**, pp. 313; c) M. Furtmair, J. Timm, R. Marschall, *Microporous Mesoporous Mater.* **2021**, *312*, 110745.
[8] C. Y. Wong, W. Y. Wong, K. Ramya, M. Khalid, K. S. Loh, W. R. W. Daud, K. L. Lim, R. Walvekar, A. A. H. Kadhum, *Int. J. Hydrogen Energy* **2019**, *44*, 6116.
[9] a) L. Nicole, C. Boissière, D. Grosso, A. Quach, C. Sanchez, *J. Mater. Chem.* **2005**, *15*, 3598; b) C. J. Brinker, Y. Lu, A. Sellinger, H. Fan, *Adv. Mater.* **1999**, *11*, 579.
[10] a) J. Timm, R. Marschall, **2018**, *2*; b) B. Yameen, A. Kaltbeitzel, A. Langer, F. Muller, U. Gosele, W. Knoll, O. Azzaroni, *Angew. Chem., Int. Ed. Engl.* **2009**, *48*, 3124.
[11] a) M. Sharifi, M. Wark, D. Freude, J. Haase, *Microporous Mesoporous Mater.* **2012**, *156*, 80; b) Y. G. Jin, S. Z. Qiao, Z. P. Xu, Z. Yan, Y. Huang, J. C. Diniz da Costa, G. Q. Lu, *J. Mater. Chem.* **2009**, *19*, 581.

[12] a) K. Lamb, R. A. Mole, D. Yu, R. de Marco, J. R. Bartlett, S. Windsor, S. P. Jiang, J. Zhang, V. K. Peterson, *Green Energy Environ.* **2017**, *2*, 294; b) J. Zeng, B. He, K. Lamb, R. De Marco, P. K. Shen, S. P. Jiang, *Chem. Commun.* **2013**, *49*, 4655.
[13] S. Fujita, A. Koiwai, M. Kawasumi, S. Inagaki, *Chem. Mater.* **2013**, *25*, 1584.
[14] R. Marschall, I. Bannat, A. Feldhoff, L. Wang, G. Q. Lu, M. Wark, *Small* **2009**, *5*, 854.
[15] J. Richard, A. Phimphachanh, J. Schneider, S. Nandi, E. Laurent, P. Lacroix-Desmazes, P. Trens, S. Devautour-Vinot, N. Marcotte, C. Gérardin, *Chem. Mater.* **2022**, *34*, 7828.
[16] J. C. Tom, C. Appel, A. Andrieu-Brunsen, *Soft Matter* **2019**, *15*, 8077.
[17] A. Khabibullin, S. D. Minteer, I. Zharov, *J. Mater. Chem. A* **2014**, *2*, 12761.
[18] R. Fan, S. Huh, R. Yan, J. Arnold, P. Yang, *Nat. Mater.* **2008**, *7*, 303.
[19] M. Zhao, Y. Liu, B. Su, *Anal. Chem.* **2019**, *91*, 13433.
[20] a) R. Brilmayer, S. Kübelbeck, A. Khalil, M. Brodrecht, U. Kunz, H. J. Kleebe, G. Buntkowsky, G. Baier, A. Andrieu-Brunsen, *Adv. Mater. Interfaces* **2020**, *7*, 1901914; b) F. M. Gilles, M. Tagliazucchi, O. Azzaroni, I. Szleifer, *J. Phys. Chem. C* **2016**, *120*, 4789.
[21] T.-C. Wei, H. W. Hillhouse, *Langmuir* **2007**, *23*, 10.
[22] D. John, M. Stanzel, A. Andrieu-Brunsen, *Adv. Funct. Mater.* **2021**, *31*, 2009732.
[23] K. Matyjaszewski, *Macromolecules* **2012**, *45*, 4015.
[24] D. R. Dunphy, P. H. Sheth, F. L. Garcia, C. J. Brinker, *Chem. Mater.* **2014**, *27*, 75.
[25] a) D. A. G. Bruggeman, *Ann. Phys.* **1935**, *416*, 636; b) J. C. Tom, R. Brilmayer, J. Schmidt, A. Andrieu-Brunsen, *Polymers* **2017**, *9*, 539.
[26] D. J. Babu, S. Yadav, T. Heinlein, G. Cherkashinin, J. J. Schneider, *J. Phys. Chem. C* **2014**, *118*, 12028.
[27] J. Bisquert, G. Garcia-Belmonte, P. Bueno, E. Longo, L. O. S. Bulhões, *J. Electroanal. Chem.* **1998**, *452*, 229.
[28] D. J. Belton, O. Deschaume, C. C. Perry, *FEBS J.* **2012**, *279*, 1710.
[29] M. Ochs, A. Khalil, T. Frömling, A. Andrieu-Brunsen, *Adv. Mater. Interfaces* **2021**, *8*, 2002095.
[30] a) M. Tagliazucchi, O. Azzaroni, I. Szleifer, *J. Am. Chem. Soc.* **2010**, *132*, 12404; b) D. Stein, M. Kruithof, C. Dekker, *Phys. Rev. Lett.* **2004**, *93*, 035901.
[31] a) C. D. Lorenz, P. S. Crozier, J. A. Anderson, A. Travesset, *J. Phys. Chem. C* **2008**, *112*, 10222; b) J. M. Rosenholm, T. Czuryszkiewicz, F. Kleitz, J. B. Rosenholm, M. Linden, *Langmuir* **2007**, *23*, 4315.
[32] S. Bazban-Shotorbani, M. M. Hasani-Sadrabadi, A. Karkhaneh, V. Serpooshan, K. I. Jacob, A. Moshaverinia, M. Mahmoudi, *J Control Release* **2017**, *253*, 46.
[33] C. H. Fujimoto, M. A. Hickner, C. J. Cornelius, D. A. Loy, *Macromolecules* **2005**, *38*, 5010.